Markov Random Field Models for Unsupervised Segmentation of Textured Color Images

Dileep Kumar Panjwani and Glenn Healey

Abstract—We present an unsupervised segmentation algorithm which uses Markov random field models for color textures. These models characterize a texture in terms of spatial interaction within each color plane and interaction between different color planes. The models are used by a segmentation algorithm based on agglomerative hierarchical clustering. At the heart of agglomerative clustering is a stepwise optimal merging process that at each iteration maximizes a global performance functional based on the conditional pseudolikelihood of the image. A test for stopping the clustering is applied based on rapid changes in the pseudolikelihood. We provide experimental results that illustrate the advantages of using color texture models and that demonstrate the performance of the segmentation algorithm on color images of natural scenes. Most of the processing during segmentation is local making the algorithm amenable to high performance parallel implementation.

Index Terms—Segmentation, color, texture, Markov random fields, machine vision, computer vision, color vision.

I. INTRODUCTION

SEGMENTATION is an important process in automated image analysis. It is during segmentation that regions of interest are extracted from an image for subsequent processing such as surface description and object recognition. There are two basic approaches to image segmentation. The first approach identifies discontinuities in some image characteristic [9], [30]. The second approach uses a similarity property for segmentation. The most common approaches in the second category are region growing [2], [6], [7], [27], region splitting [21], and region splitting and merging [24]. Recently, researchers have shown interest in using color images for segmentation [1], [13], [17] and several important benefits of using color have been identified [14].

In many applications in image processing and analysis, spatial-interaction models especially the conditional Markov models are useful for modeling textures [3], [4], [15], [19]. The modeling of color textures, however, has received less attention. In this paper, we present Gaussian Markov random field (GMRF) models for color textures and use these models for color image segmentation. The Gaussian Markov random fields are a special case of the Markov random fields (MRFs) [3], [28] and have been shown to be an accurate compact representation for a range of textures [4], [7]. These models have

been studied extensively [15], [28]. In this work, we study the use of these models for representing color images described by a red, green, blue (RGB) vector at each pixel. Alternatively, a color image is sometimes referred to as the combination of red, green, and blue color planes. The model we develop describes a color texture in terms of the statistical dependence of the RGB vector measured at a pixel on the RGB values measured at neighboring pixels. Several previous color texture models are discussed in [11] with emphasis on efficient representations for perceptually accurate texture synthesis. Color textures have also been represented using region boundaries at multiple scales [26].

Several approaches to supervised maximum a posteriori probability (MAP) segmentation using Markov random fields are based on the methodology introduced by Geman and Geman [12]. This formulation exploits the equivalence between MRFs and Gibbs distributions with images modeled using an intensity process and a line process. The model parameters that describe the Gibbs distribution in image regions are assumed a priori known. Finding the maximum of the posterior distribution requires a computationally intensive optimization which is computed in [12] using stochastic annealing. Other researchers [25], [10], [29] have extended this approach to coupled MRFs that consider additional cues such as color, stereo, and motion. In [25], hue is the only color feature used. All three color bands are considered in [10] and [29], but the interdependence between color bands is only considered at boundaries.

In the years since the work of Geman and Geman [12], several researchers have addressed the more difficult problem of unsupervised segmentation for which no prior knowledge of texture parameters is assumed. Most of these techniques assume an image model and estimate model parameters before using a clustering scheme to arrive at the segmented image [8], [20], [27]. Other researchers have used a simultaneous estimation and segmentation approach to the problem [18]. While the underlying approaches are quite powerful, these unsupervised segmentation algorithms have only been applied to gray scale images of a limited class of scenes.

The segmentation algorithm developed in this paper is region-based and uses color GMRF models. We do not explicitly use edge finding processes because these processes are often confused by intensity variation within textured regions or by texture boundaries that are not accompanied by prominent intensity boundaries. The algorithm consists of a region splitting phase and an agglomerative clustering phase. In the region splitting phase, the image is partitioned into a number of square regions that are recursively split until each region satis-

fies a uniformity criterion. The agglomerative clustering phase is divided into a conservative merging process followed by a stepwise optimal merging process. Conservative merging uses color mean and covariance estimates and a criterion based on the similarity of color textures for the efficient processing of local merges. Following conservative merging, a stepwise optimal merging process based on a global performance functional is used to complete the segmentation. The global performance functional is the conditional pseudolikelihood of the image given the regions and estimated color GMRF parameters. The stepwise optimal merging process is stopped using a test based on rapid changes in the pseudolikelihood of the image. This algorithm has been applied to several color images of natural scenes.

II. GAUSSIAN MARKOV RANDOM FIELDS FOR COLOR TEXTURES

For gray level images, spatial interaction models characterize statistical dependence by representing the intensity at each pixel as a linear combination of neighboring intensities and additive noise. For a given pixel, neighboring pixels are defined by a neighbor set N. Thus, the intensity $I(i, j)$ at pixel (i, j) is represented as a linear combination of the pixel intensities $\{I(i + m, j + n), (m, n) \in N\}$ plus correlated noise. If N is defined as $N = \{(m, n) : m \leq 0, n \leq 0, (m, n) \neq (0, 0)\}$, the model obtained will be causal. Noncausal models which allow more general neighbor sets are more powerful for modeling images. For example, a noncausal first order model is defined by the four neighbors $N = \{(0, -1), (0, 1), (-1, 0), (1, 0)\}$.

A model used for representing color textures should take into account not only the spatial interaction within each of the three color planes, but also the interaction between different color planes. Thus, for color images each component of the RGB vector at location (i, j) will be represented as a linear combination of the color components of the neighbors and additive noise. This can be achieved by selecting a neighborhood structure that models both within-plane and across-plane interactions. For example, the neighbor set defining spatial interaction of a red measurement with the red color components of neighbors is denoted N_{rr}, while another set defining its interaction with the green color components of its neighbors is N_{rg}. A complete representation uses nine 2D neighborhood matrices defining the interactions between each pair of color planes.

A. Model Representation

Let $C(i, j) = [R(i, j)\ G(i, j)\ B(i, j)]$ represent a color pixel at location (i, j) in a textured region S. Let μ_R, μ_G, and μ_B denote mean color intensities. If we use a GMRF to model the textured region, the conditional probability density function of C(i, j) will be given by

$$P(C(i, j)| S) =$$

$$\frac{1}{(8\pi^3 |\Sigma|)^{\frac{1}{2}}} exp\left\{-\frac{1}{2}[e_r(i, j)e_g(i, j)e_b(i, j)]\Sigma^{-1}[e_r(i, j)e_g(i, j)e_b(i, j)]^t\right\}$$

(1)

where $[e_r(i, j)\ e_g(i, j)\ e_b(i, j)]$ is a zero mean Gaussian noise vector and where

$$\Sigma = \begin{bmatrix} V_{rr} & V_{rg} & V_{rb} \\ V_{gr} & V_{gg} & V_{gb} \\ V_{br} & V_{bg} & V_{bb} \end{bmatrix}$$

(2)

denotes the noise correlation matrix with V_{pq} the expected value of $e_p\ e_q$. The spatial interaction of the color pixels is represented by

$$e_r(i, j) = (R(i, j) - \mu_R) - \sum_{(m,n) \in N_{rr}} \alpha_{RR}(m, n)(R(i+m, j+n) - \mu_R)$$

$$- \sum_{(m,n) \in N_{rg}} \alpha_{RG}(m, n)(G(i+m, j+n) - \mu_G)$$

$$- \sum_{(m,n) \in N_{rb}} \alpha_{RB}(m, n)(B(i+m, j+n) - \mu_B)$$

(3)

$$e_g(i, j) = (G(i, j) - \mu_G) - \sum_{(m,n) \in N_{gr}} \beta_{GR}(m, n)(R(i+m, j+n) - \mu_R)$$

$$- \sum_{(m,n) \in N_{gg}} \beta_{GG}(m, n)(G(i+m, j+n) - \mu_G)$$

$$- \sum_{(m,n) \in N_{gb}} \beta_{GB}(m, n)(B(i+m, j+n) - \mu_B)$$

(4)

$$e_b(i, j) = (B(i, j) - \mu_B) - \sum_{(m,n) \in N_{br}} \gamma_{BR}(m, n)(R(i+m, j+n) - \mu_R)$$

$$- \sum_{(m,n) \in N_{bg}} \gamma_{BG}(m, n)(G(i+m, j+n) - \mu_G)$$

$$- \sum_{(m,n) \in N_{bb}} \gamma_{BB}(m, n)(B(i+m, j+n) - \mu_B)$$

(5)

where the αs, βs, and γs are the model parameters and the subscripted N sets define the different neighborhood matrices. Thus, the color vector at each location (i, j) is a linear combination of neighbors in all three color planes plus Gaussian noise. Fig. 1 represents the spatial interaction model graphically by showing how a pixel $R(i, j)$ in the red plane interacts with three neighbors in the red and blue planes through α parameters.

B. Parameter Estimation

Parameter estimation is a classical problem in statistics and it can be approached in several ways. In this paper, we develop a segmentation algorithm which uses agglomerative clustering directed by a criterion which is based on the likelihood of the image. For this reason, we consider maximum likelihood (ML) methods for parameter estimation. The goal of these methods is to produce maximum likelihood estimates for the parameters of a color GMRF model for a given image region S.

B.1. Code Method

A code S_C is a certain set of pixels in a region among which there is no spatial interaction [3]. The likelihood of the code
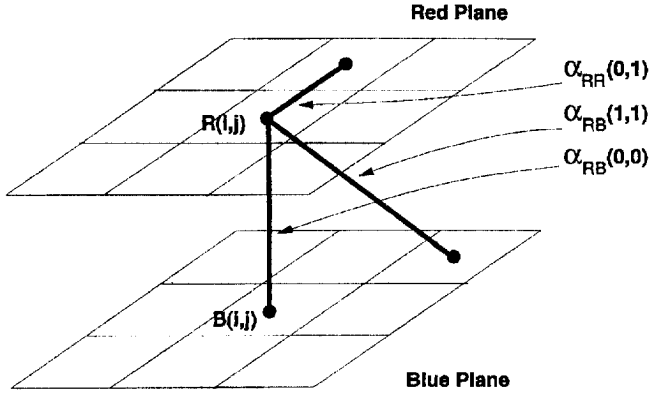
Red Plane

Fig. 1. Modeling spatial interaction in color images.

will be the function

$$\prod_{(i,j)\in S_C} \frac{1}{\left(8\pi^3|\Sigma_{S_C}|\right)^{\frac{1}{2}}} exp\left\{-\frac{1}{2}\left[e_r(i, j)e_g(i, j)e_b(i, j)\right]\Sigma_{S_C}^{-1}\left[e_r(i, j)e_g(i, j)e_b(i, j)\right]^t\right\}$$

(6)

where Σ_{S_C} is the noise correlation matrix corresponding to the code S_C.

We can estimate the α, β, and γ parameters in (3), (4), and (5) by maximizing this likelihood function. For intensity images, such estimation can be achieved by solving a set of linear equations [15]. For color images modeled using a total of m of the α, β, and γ parameters the estimation requires the solution of a set of ($m + 6$) nonlinear equations with the extra six equations required for the estimation of the independent elements of Σ_{S_C}. An important limitation of code estimates is that they are not efficient due to partial utilization of the data [15]. In addition, code estimates are not unique and estimates obtained using different codes can differ considerably [15].

B.2. Pseudolikelihood Method

For a region S modeled by a GMRF, the function

$$\prod_{(i,j)\in S} \frac{1}{\left(8\pi^3|\Sigma_S|\right)^{\frac{1}{2}}} exp\left\{-\frac{1}{2}\left[e_r(i, j)e_g(i, j)e_b(i, j)\right]\Sigma_S^{-1}\left[e_r(i, j)e_g(i, j)e_b(i, j)\right]^t\right\}$$

(7)

is the product of conditional probability densities of each pixel in S. Since a color vector $[R(i, j)\ G(i, j)\ B\ (i, j)]$ is dependent on its neighbors according to (3), (4), and (5), neighboring color vectors are not statistically independent. Thus, the product of conditional probabilities in (7) is not a true likelihood. This function is often called the pseudolikelihood of the region. The estimates obtained by maximizing the pseudolikelihood have been shown to be efficient and consistent [15]. The equations used for computing pseudolikelihood estimates are identical to those for the code estimates except that all of the data is used.

B.3. Fourier Transform Method

Code and pseudolikelihood methods for ML parameter estimation do not use the true likelihood of the data. It is difficult to compute the joint probability density of the pixels in a re-

gion due to the spatial interaction among them. However, the Jacobian of the transformation from the image data to its discrete Fourier transform (DFT) is unity [16]. Therefore, the sets of parameters obtained by maximizing the likelihood of a region and the likelihood of the DFT of the region are the same.

For an infinitely large region S, components of the DFT are independent and have a gaussian distribution. This allows the derivation of an expression for the likelihood of the DFT of the image data [16]. The likelihood function of the DFT is a complicated function of the parameters of the GMRF model. By using a doubly periodic extension of the finite lattice region (toroidal lattice), however, explicit expressions for the log-likelihood function of an image region can be obtained [5]. The maximization of this likelihood requires using nonlinear optimization procedures such as gradient methods for parameter estimation.

III. SEGMENTATION ALGORITHM

We have implemented a segmentation algorithm that uses the color GMRF model presented in Section II. The segmentation process is divided into a region splitting phase and an agglomerative clustering phase. The agglomerative clustering phase consists of conservative merging followed by stepwise optimal merging. The region splitting phase is used to ensure that initial image segments are small enough to fall within a single textured region in the image. Conservative merging proceeds locally to merge similar adjacent regions. Stepwise optimal merging completes the segmentation by iteratively processing optimal merges until a stopping criterion is satisfied. We illustrate the results of each stage of the algorithm on an image of a wall of the Grand Canyon containing a rock and a tree (Fig. 2).

Fig. 2. Image of a rock and tree.

A. Region Splitting

A clustering procedure partitions data into groups or clusters that possess strong similarities. Before applying a clustering procedure using the image model described in Section II.A, each image segment must be assumed to be uniform in the sense that it contains a single texture described by a color GMRF model. Ideally, at the start of the clustering process

each pixel might be considered as a separate cluster. For two reasons, this is not feasible. First, if the image is large the segmentation process will become computationally expensive. Second, the criterion used for merging requires some minimum number of pixels in an image segment to estimate the GMRF parameters.

To form initial uniform image segments, the input image is first divided into a number of square blocks. The starting block size should be small to minimize the possibility of including more than one texture within a block. However, since the goal of region splitting is to generate regions that can be input to a clustering procedure that merges based on color texture properties, the initial square blocks are of the minimum size for which the GMRF parameters can be estimated reliably. Each block is considered as a sample to test for uniformity or nonuniformity. If the sample satisfies the nonuniformity hypothesis then the block is split into four subblocks and the procedure is repeated recursively on each subblock until blocks reach a minimum size of 4×4 pixels. A possible error occurs when a block of a single texture is split into four, but this error can be corrected during agglomerative clustering later in the segmentation process. On the other hand, when blocks containing more than one texture are assumed to be uniform, then error recovery is not possible.

The uniformity test is based on an analysis of estimated color mean vectors and covariance matrices. Let S be a small image segment. There are two possible hypotheses that can be tested: H_0, the region is uniform and H_1, the region is nonuniform. Using a test similar to the one developed in [6], an image block S is assumed to be uniform if each component of its estimated color mean $\mu_S = [\mu_R \ \mu_G \ \mu_B]$ differs by less than a threshold ϵ_μ from the estimated color mean for each of its four subblocks S_1, S_2, S_3, and S_4 and if each of the six unique components of its estimated covariance matrix $E \{[R - \mu_R, G - \mu_G, B - \mu_B]^T [R - \mu_R, G - \mu_G, B - \mu_B]\}$ also differ by less than a threshold ϵ_σ from the corresponding elements of the estimated covariance matrices for S_1, S_2, S_3, and S_4. To avoid the presence of nonuniform blocks following region splitting, the thresholds are kept small. Fig. 3 shows the partitioning of Fig. 2 after the region splitting phase of the segmentation process. Note that all potentially nonuniform blocks have been recursively split until a minimum size of 4×4 is reached.
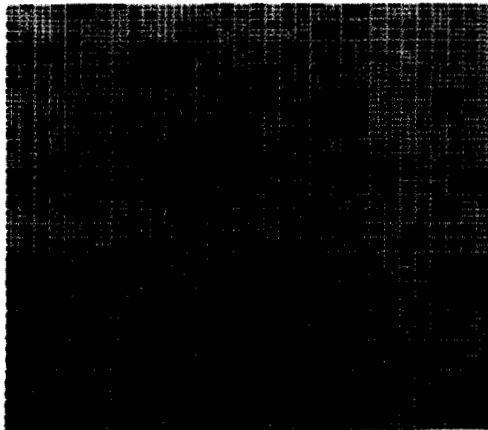

Fig. 3. Result after the region splitting phase.

B. Agglomerative Hierarchical Clustering

One way to begin a clustering procedure is to define a suitable distance function and compute the matrix of distances between all pairs of samples. If this distance is a good measure of dissimilarity, then the distance between samples that belong in the same cluster should be significantly less than the distance between other pairs of samples. As described in III.A, region splitting is used to partition an image into initial segments with every segment considered a cluster. In this section, we describe the use of a subsequent agglomerative hierarchical clustering phase consisting of conservative merging and stepwise optimal merging. For image segmentation, the clustering procedure may only merge clusters corresponding to image segments which are spatially adjacent to one another. We begin in III.B.1 by describing the function that will be used to measure the similarity of textured color regions.

B.1. The Pseudolikelihood Ratio for Directing Clustering

The criterion that we use for clustering is based on the pseudolikelihood of the image and is similar to an approach used by Silverman and Cooper [27]. It is difficult to find the true likelihood of the image in the spatial domain. Approximate methods use the code likelihood or the pseudolikelihood as described in Section II.B. Coding methods do not utilize the data completely and the parameter estimates are not efficient. Using the pseudolikelihood for developing the merging criterion allows consistent parameter estimation and complete utilization of the image data [15]. An alternative global performance functional is the likelihood of the discrete Fourier transform of the image data.

For the color GMRF model discussed in Section II, let θ_S be the vector of μ_R, μ_G, μ_B, and the α, β, and γ parameters used in (3), (4), and (5) to describe image data in a region S. At some stage in the clustering process, let the image consist of segments S_1, S_2, $\cdots$, S_Q. Consider two spatially adjacent image segments S_k and S_l modeled using color Gaussian markov random fields with pseudolikelihood parameter estimates $(\theta_{S_k}, \Sigma_{S_k})$ and $(\theta_{S_l}, \Sigma_{S_l})$. Let S_M be the new image segment obtained by merging S_k and S_l and let S_M be modeled by pseudolikelihood parameters $(\theta_{S_M}, \Sigma_{S_M})$. Let $P_{ps}(S \mid \theta_S, \Sigma_S)$ be the pseudolikelihood of a segment S given the parameters θ_S and Σ_S. The ratio R_{ps} of the pseudolikelihood of the image before the merge and the pseudolikelihood of the image after the merge is

$$R_{ps}(k, l) = \frac{\prod\limits_{r=1,2,\ldots Q:} P_{ps}\left(S_r \middle| \theta_{S_r}, \Sigma_{S_r}\right)}{P_{ps}\left(S_M \middle| \theta_{S_M}, \Sigma_{S_M}\right) \prod\limits_{r=1,2,\ldots,Q; r \neq k,l} P_{ps}\left(S_r \middle| \theta_{S_r}, \Sigma_{S_r}\right)} \quad (8)$$

This expression simplifies to

$$R_{ps}(k, l) = \frac{P_{ps}\left(S_k \middle| \theta_{S_k}, \Sigma_{S_k}\right) P_{ps}\left(S_l \middle| \theta_{S_l}, \Sigma_{S_l}\right)}{P_{ps}\left(S_M \middle| \theta_{S_M}, \Sigma_{S_M}\right)} \quad (9)$$

Values of $R_{ps}(k, l)$ near one indicate S_k and S_l have similar color textures while larger values of $R_{ps}(k, l)$ suggest S_k and S_l have dissimilar color textures.

As described in Section II.B.2, if the GMRF used for modeling has m parameters, then $m + 6$ nonlinear equations must be solved to estimate parameters for a region S. If the GMRF model chosen for a texture fits well, however, the terms e_r, e_g, and e_b will behave like pure noise independent of the properties of the underlying texture. We have shown experimentally [22] that as the GMRF model becomes more accurate for a range of textures the estimated nondiagonal correlations among e_r, e_g, and e_b in (2) become small. In order to improve the efficiency of the image segmentation algorithm, we assume that the nondiagonal terms in Σ are zero. This assumption leads to a system of linear equations for parameter estimation. These equations are presented in Appendix A.

To simplify the computation of (9), we define a function $h(k, l)$ which is the log of the pseudolikelihood ratio $h(k, l) = \ln(R_{ps}(k, l))$. In Appendix B, we show that for the model discussed in Section II using the parameter estimation scheme derived in Appendix A, $h(k, l)$ simplifies to

$$h(k, l) = \frac{(D_k + D_l)}{2}\ln(|\Sigma_{S_M}|) - \frac{D_k}{2}\ln(|\Sigma_{S_k}|) - \frac{D_l}{2}\ln(|\Sigma_{S_l}|) \quad (10)$$

where D_k and D_l are the numbers of pixels in segments S_k and S_l. To develop a similar function using likelihood in the Fourier transform domain requires the parameter estimation technique described in Section II.B.3. Since initial image segments are often small in the segmentation process, the underlying toroidal lattice assumption of this parameter estimation method is often not a good approximation. In addition, this method requires nonlinear optimization for parameter estimation which would make the clustering process expensive computationally. For these reasons, we use the log pseudolikelihood ratio of (10) to direct clustering during segmentation.

B.2. Conservative Merging

The result of region splitting is to divide the image into uniform segments. Some of these segments will be small, particularly in the vicinity of region boundaries. The pseudolikelihood ratio developed in Section III.B.1 cannot be applied to small regions since there are insufficient pixels to estimate the GMRF parameters. It is desirable for computational efficiency to minimize the number of initial clusters input to the final stepwise optimal merging stage since this stage requires choosing the best merge over the entire image. In consideration of these factors a local conservative merging is applied to adjacent image segments following region splitting.

Two criteria are used to guide the conservative merging process. First, the differences in each element of the color mean vector and covariance matrix for adjacent regions must be below a threshold vector in a way similar to the test described in Section III.A for region splitting. Second, the pseudolikelihood ratio of (9) for the merge must be less than a threshold. If the size of a segment is smaller than the minimum required for reliable estimation of the pseudolikelihood ratio, then only the first criterion is used. In order to estimate reliably the GMRF parameters and

compute the pseudolikelihood ratio, we require a segment to have at least twice as many pixels as the number of parameters to be estimated. To avoid the possibility of errors during conservative merging, small thresholds are used for each test. If there is more than one neighboring segment of any segment for which a conservative merge is appropriate, then the merge is processed with the segment having the smallest Euclidean distance in color mean. This process is repeated until any possible new merge does not satisfy the conservative merging criteria. Fig. 4 is the result of applying the conservative merging process to the intermediate result in Fig. 3. At this stage, most of the image segments have grown large enough to allow the estimation of GMRF parameters and no incorrect merges have been processed. Another observable feature is the formation of boundaries between dissimilar textures.
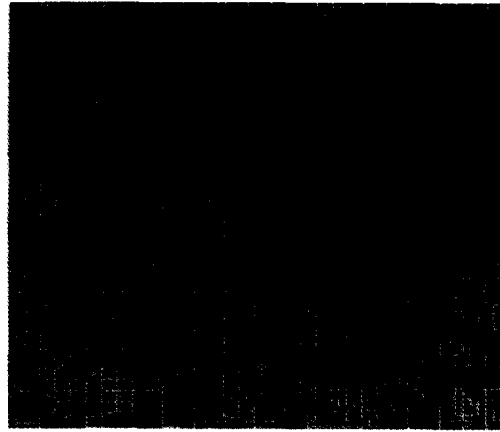

Fig. 4. Result after the conservative merging phase.

B.3. Stepwise Optimal Merging

Following conservative merging, stepwise optimal merging is used to complete the segmentation. The criterion directing stepwise optimal merging is to merge two spatially adjacent image segments S_k and S_l if

$$h(k, l) = \min_{i,j} h(i, j) \quad (11)$$

where i and j vary over all adjacent pairs of segments S_i and S_j in the image and where $h(k, l)$ is defined by (10). Thus, at each step this procedure finds the pair of adjacent clusters whose merger would decrease the conditional pseudolikelihood of the image given the clusters as little as possible. This assures us that at each iteration the algorithm selects the best possible merge, even if it does not guarantee that the resulting segmentation will provide the optimal partitioning of the image.

During stepwise optimal merging some image segments may still be small enough so that the pseudolikelihood ratio for a merge cannot be computed reliably and the criterion (11) cannot be applied to these regions. To consider small segments during the merging process, we use a modified criterion for directing stepwise optimal merging. The modified criterion requires two steps. The criterion (11) is used to find the best merge $bestmerge1$ among pairs of segments which are sufficiently large. The Euclidean color mean distance is computed

for each possible merge involving at least one image segment which is small and the best merge using this test is called *bestmerge2*. If the color mean difference for *bestmerge2* is smaller than the color mean difference for *bestmerge1*, then *bestmerge2* is selected as the best merge. Otherwise, *bestmerge1* is selected as the best merge. The stopping rule to be described below is applied only after segments are merged according to *bestmerge1*.

Stepwise optimal merging continues until the stopping rule succeeds. Let there be a set of p clusters at some stage of clustering and let S_i and S_j be the best pair of clusters for merging using the criterion (11). A decision must be made whether these two clusters should be merged to obtain a new cluster set or whether the segmentation process should be stopped. The merging of regions corresponding to different textures results in a large decrease in the likelihood of an image and a corresponding large value for the pseudolikelihood ratio R_{ps} of (8). A stopping rule can be developed based on changes in the pseudolikelihood ratio.

We develop a test which stops merging if the pseudolikelihood ratio corresponding to a new merge is large compared to the pseudolikelihood ratio for the last merge. If R_{ps}^l is the pseudolikelihood ratio of the image for the last merge and R_{ps}^n is the pseudolikelihood ratio of the image for the new merge, this test can be stated as: Stop clustering if

$$\left(\ln R_{ps}^n - \ln R_{ps}^l\right) > T \tag{12}$$

where T is a constant. The difficulty associated with this test is to determine T. If the image contains few regions and most of these regions are large, then this test works well and segmentation results are relatively insensitive to the choice of T. This is because, for this case, the decrease in the likelihood of the image for merging regions corresponding to different textures will be large. On the other hand, if an image consists of many small regions with different textures, this may not be the case. In [22], we derive a likelihood ratio test for stopping clustering that uses the likelihood of the image in the Fourier transform domain. This test is significantly more computationally expensive than (12). For the experiments presented in Section IV, this likelihood ratio test was applied when the stopping test of (12) succeeded. If both tests succeeded, then clustering was stopped. Fig. 5 is the final segmentation resulting from stepwise optimal merging with Fig. 6 a plot of the pseudolikelihood ratio at each merge. Both stopping tests succeeded following the 121st merge. There are five peaks in the graph and at each peak the second stopping rule was invoked. The GMRF parameters for the rock and tree textures in the segmented image are shown in Table I. The associated bar graphs display the magnitude of the tabulated parameters with shaded bars indicating within-plane interactions. Note that several parameters describing across-plane interactions are quite large.
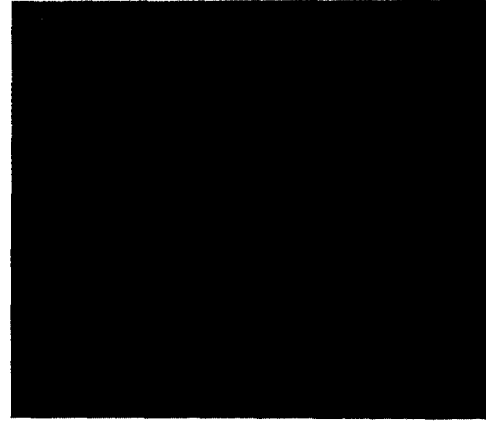

Fig. 5. Result after the stepwise optimal merging phase.

TABLE I
THE GMRF PARAMETERS FOR TEXTURES IN FIG. 2

| Parameter	Rock	Tree
$\alpha_{RR}(1,0)$	0.2998	0.3378
$\alpha_{RR}(0,1)$	0.2194	0.0540
$\alpha_{RR}(1,1)$	-0.1739	0.0854
$\alpha_{RR}(1,-1)$	0.1107	-0.1405
$\alpha_{RG}(1,0)$	0.0303	0.1319
$\alpha_{RG}(0,1)$	0.0595	0.1109
$\alpha_{RG}(1,1)$	-0.0460	0.1254
$\alpha_{RG}(1,-1)$	-0.0598	0.0209
$\alpha_{RB}(1,0)$	0.0125	0.0401
$\alpha_{RB}(0,1)$	0.0179	0.1928
$\alpha_{RB}(1,1)$	0.0227	-0.0798
$\alpha_{RB}(1,-1)$	0.0165	-0.1148
$\beta_{GG}(1,0)$	0.5302	0.3714
$\beta_{GG}(0,1)$	0.1155	0.0053
$\beta_{GG}(1,1)$	-0.1291	0.0417
$\beta_{GG}(1,-1)$	-0.0255	-0.0495
$\beta_{GR}(1,0)$	-0.1205	0.1863
$\beta_{GR}(0,1)$	0.1263	0.1561
$\beta_{GR}(1,1)$	-0.0730	-0.1226
$\beta_{GR}(1,-1)$	0.0940	-0.0453
$\beta_{GB}(1,0)$	-0.0603	-0.0300
$\beta_{GB}(0,1)$	0.0673	0.1560
$\beta_{GB}(1,1)$	-0.0030	-0.0398
$\beta_{GB}(1,-1)$	- 0.0058	-0.1297
$\gamma_{BB}(1,0)$	0.3795	0.4937
$\gamma_{BB}(0,1)$	0.2665	0.1400
$\gamma_{BB}(1,1)$	-0.1702	0.0442
$\gamma_{BB}(1,-1)$	-0.0302	-0.1879
$\gamma_{BR}(1,0)$	-0.0236	0.0207
$\gamma_{BR}(0,1)$	0.0952	0.1310
$\gamma_{BR}(1,1)$	-0.0579	-0.0173
$\gamma_{BR}(1,-1)$	0.0644	- 0.0620
$\gamma_{BG}(1,0)$	-0.0013	0.0019
$\gamma_{BG}(0,1)$	-0.0541	0.0783
$\gamma_{BG}(1,1)$	0.0249	-0.0920
$\gamma_{BG}(1,-1)$	0.0260	0.0113
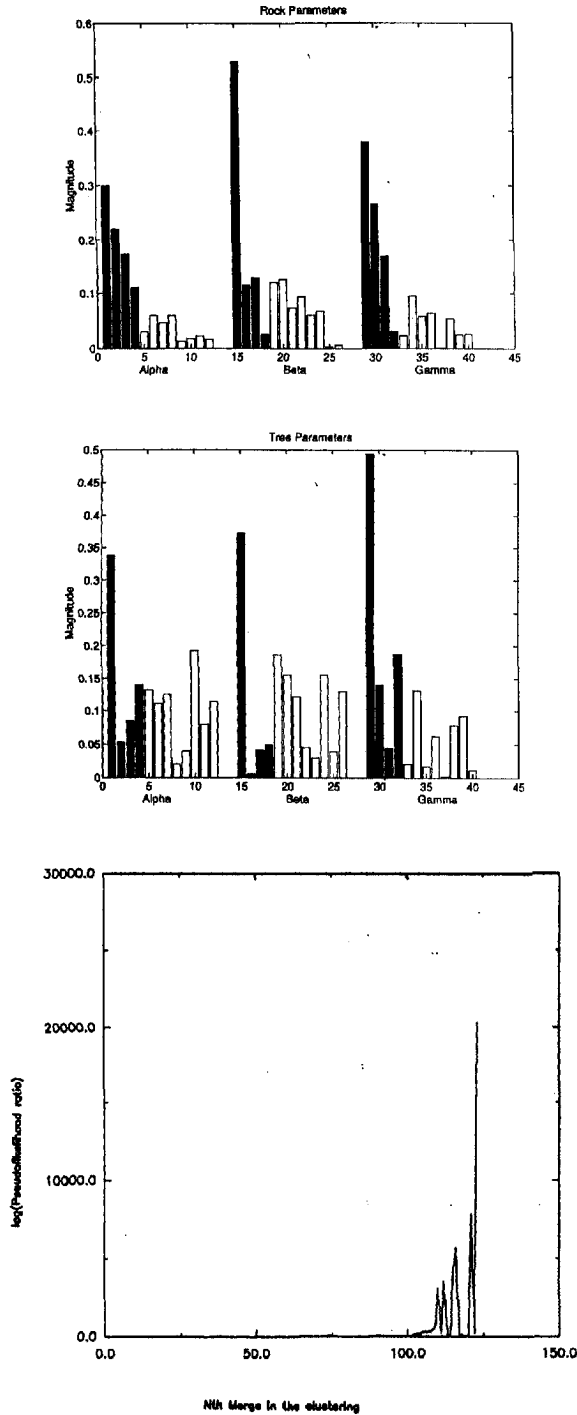
Fig. 6. Graph of the pseudolikelihood ratio at each merge.

IV. EXPERIMENTAL RESULTS

We conducted a set of experiments to study the properties of the color GMRF model and the segmentation algorithm. The results in Section IV.A show that the use of a color texture model can significantly improve the results of texture segmentation over purely intensity-based methods. In Section IV.B, we present experimental results obtained by applying the unsupervised segmentation algorithm developed in Section III to several color images of natural scenes.

A. Comparison of Different Models

Fig. 7 is an image of four textures T_1 (upper left), T_2 (upper right), T_3 (lower left), and T_4 (lower right) corresponding to different red papers. Since the image contains a small number of large regions, we used only the agglomerative clustering phase of the segmentation algorithm. The red textures in Fig. 7 have similar color mean values $[\mu_R, \mu_G, \mu_B]$ given by $T_1 = [229.6 \quad 33.4 \quad 13.0]$, $T_2 = [228.5 \quad 32.8 \quad 13.7]$, $T_3 = [131.9 \; 44.2 \; 18.6]$, and $T_4 = [226.2 \; 31.1 \; 24.1]$. Thus, the segmentation will be governed primarily by the textural properties of the regions. We first applied the segmentation algorithm to the intensity image. The neighborhood matrix N used for the second order GMRF model was

$$N = \begin{bmatrix} 4 & 2 & 3 \\ 1 & 0 & 1 \\ 3 & 2 & 4 \end{bmatrix} \tag{13}$$

where nonzero integers in the matrix indicate the locations of neighbors. One GMRF parameter is used to represent interaction between the center location and all locations labeled with the same integer. The image is of size 256×256 and the initial size of each region was set to 16×16. Fig. 8 shows the result of the segmentation.
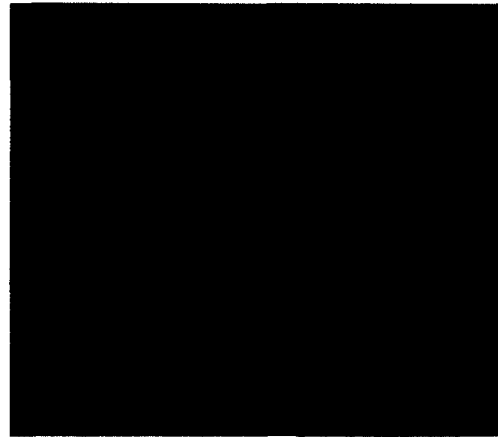
Fig. 7. Image of four red textures.

Fig. 8. Result of the segmentation using the intensity model.

The segmentation algorithm was subsequently applied to the color image using a second order color GMRF model M_1 which takes into account interaction within each color plane using three structurally equivalent neighborhood matrices $N_{rr} = N_{gg} = N_{bb}$ with each taking the structure of N in (13). Thus, there are a total of 12 within-plane parameters and zero across-plane parameters. Fig. 9 shows the result of the segmentation using the second order color GMRF model M_1.

Fig. 9. Result of the segmentation using the color model M_1.

The same segmentation algorithm was also applied using a second order color GMRF model M_2 which takes into account interaction within each color plane using three structurally equivalent neighborhood matrices $N_{rr} = N_{gg} = N_{bb}$ and takes into account interaction between color planes using six structurally equivalent neighborhood matrices $N_{rg} = N_{rb} = N_{gr} = N_{gb} = N_{br} = N_{bg}$

$$N_{rr} = \begin{bmatrix} 4 & 2 & 3 \\ 1 & 0 & 1 \\ 3 & 2 & 4 \end{bmatrix} \quad N_{rg} = \begin{bmatrix} 8 & 6 & 7 \\ 5 & 0 & 5 \\ 7 & 6 & 8 \end{bmatrix} \quad (14)$$

Thus, there are a total of 12 within-plane parameters and 24 across-plane parameters. Fig. 10 shows the result of the segmentation using the second order color GMRF model M_2. Fig. 11 is a plot of the log pseudolikelihood ratio of (11) for each merge processed during stepwise optimal merging. The stopping rule terminated clustering before the 61st merge. Fig. 11 indicates a large increase in (11) at the 61st merge. A threshold $T = 200$ was used with the stopping rule.

The segmentation algorithm based on the intensity model partitions the image into five regions as shown in Fig. 8. A large part of texture T_2 has been merged with T_4. This occurs because the intensity texture model is not sufficient to represent the textural variations. The segmented image using the model M_1 contains four regions with a small part of T_2 being merged with T_4. The algorithm based on the color model M_2, which uses the neighborhood matrices to take into account within-plane and across-plane interactions, segments all four textures accurately. We list the color GMRF parameters estimated using the M_2 model for each texture in Table II. The associated bar graphs display the magnitude of the tabulated parameters with shaded bars indicating within-plane interac-

tions. The parameters estimated for within-plane interactions and across-plane interactions can be quite different. For example, for T_2 all across-plane interaction parameters are small. For T_3, the γ_{BG} parameters are significantly larger. The results in Figs. 9 and 10 show that for this image the use of across-plane interaction parameters leads to a small improvement in segmentation performance. For textures with more significant pixel-to-pixel color variation, the importance of across-plane interactions becomes more evident. In [23], we address the general problem of selecting appropriate neighbor sets for color random field models and present examples where the use of across-plane interaction parameters significantly improves segmentation results.
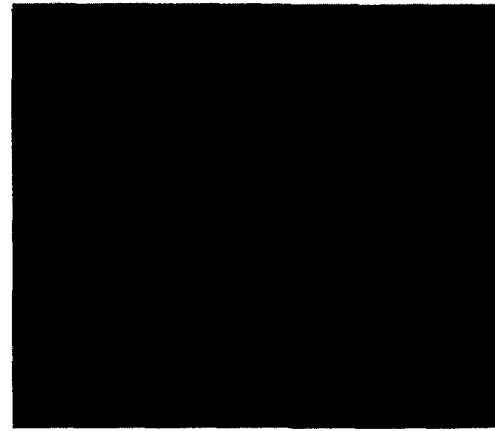

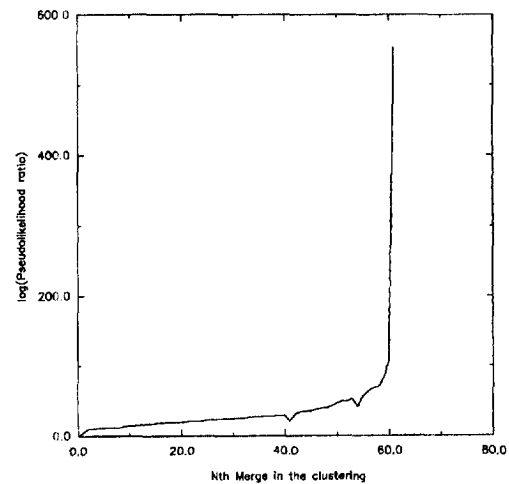Fig. 10. Result of the segmentation using the color model M_2.


Fig. 11. Graph of the pseudolikelihood ratio at each merge.

B. Results on Images of Natural Scenes

In this section, we present results generated by the segmentation algorithm on a variety of color images of natural scenes. The same set of parameter values and thresholds was used for processing all of the images in this section as well as the image in Section III. During the region splitting phase, we used $\epsilon_\mu = 10$ for the mean comparison test and $\epsilon_\sigma = 36$ for the covariance comparison test. In the conservative merging phase,

TABLE II
THE GMRF PARAMETERS FOR FOUR RED TEXTURES IN FIG. 7

Parameter	T_1	T_2	T_3	T_4
$\alpha_{RR}(1,0)$	0.4420	0.3552	0.4401	0.4301
$\alpha_{RR}(0,1)$	0.2246	0.0640	0.0645	-0.0040
$\alpha_{RR}(1,1)$	-0.0865	0.0103	0.0003	0.0129
$\alpha_{RR}(1,-1)$	-0.0875	0.0204	-0.0615	0.0471
$\alpha_{RG}(1,0)$	0.0266	0.0218	0.0751	-0.0281
$\alpha_{RG}(0,1)$	0.0387	-0.0021	0.0696	-0.0008
$\alpha_{RG}(1,1)$	-0.0080	0.0060	-0.0464	0.0109
$\alpha_{RG}(1,-1)$	-0.0074	-0.0132	-0.0366	-0.0085
$\alpha_{RB}(1,0)$	0.0268	0.0274	0.0301	0.0314
$\alpha_{RB}(0,1)$	0.0575	0.0189	0.0432	0.0225
$\alpha_{RB}(1,1)$	-0.0408	-0.0116	-0.0181	-0.0146
$\alpha_{RB}(1,-1)$	-0.0622	-0.0234	-0.0463	-0.0249
$\beta_{GG}(1,0)$	0.2687	0.2777	0.3833	0.1518
$\beta_{GG}(0,1)$	0.1279	0.0920	0.1755	-0.0050
$\beta_{GG}(1,1)$	0.0010	-0.0016	-0.0310	0.0597
$\beta_{GG}(1,-1)$	-0.0020	-0.0262	-0.0585	0.0403
$\beta_{GR}(1,0)$	0.0307	0.0209	0.0331	-0.0035
$\beta_{GR}(0,1)$	0.0318	0.0031	-0.0028	-0.0011
$\beta_{GR}(1,1)$	-0.0107	0.0067	0.0098	0.0004
$\beta_{GR}(1,-1)$	-0.0159	-0.0168	-0.0241	-0.0086
$\beta_{GB}(1,0)$	0.0724	0.0374	0.0490	0.1207
$\beta_{GB}(0,1)$	0.0521	0.0201	0.0461	0.0330
$\beta_{GB}(1,1)$	-0.0255	-0.0017	-0.0349	-0.0152
$\beta_{GB}(1,-1)$	-0.0308	-0.0033	-0.0347	0.0012
$\gamma_{BB}(1,0)$	0.4171	0.4134	0.4824	0.4311
$\gamma_{BB}(0,1)$	0.2231	0.0590	0.1326	0.0844
$\gamma_{BB}(1,1)$	-0.0659	-0.0164	-0.0278	-0.0331
$\gamma_{BB}(1,-1)$	-0.0577	-0.0062	-0.0689	-0.0061
$\gamma_{BR}(1,0)$	0.0309	0.0365	0.0262	0.0251
$\gamma_{BR}(0,1)$	0.0634	0.0245	0.0082	0.0255
$\gamma_{BR}(1,1)$	-0.0365	-0.0130	0.0120	-0.0145
$\gamma_{BR}(1,-1)$	-0.0663	-0.0340	-0.0670	-0.0382
$\gamma_{BG}(1,0)$	0.0845	0.0351	0.0765	0.0895
$\gamma_{BG}(0,1)$	0.0680	0.0436	0.1527	0.0211
$\gamma_{BG}(1,1)$	-0.0567	-0.0022	-0.1147	0.0008
$\gamma_{BG}(1,-1)$	-0.0701	-0.0210	-0.0866	0.0037
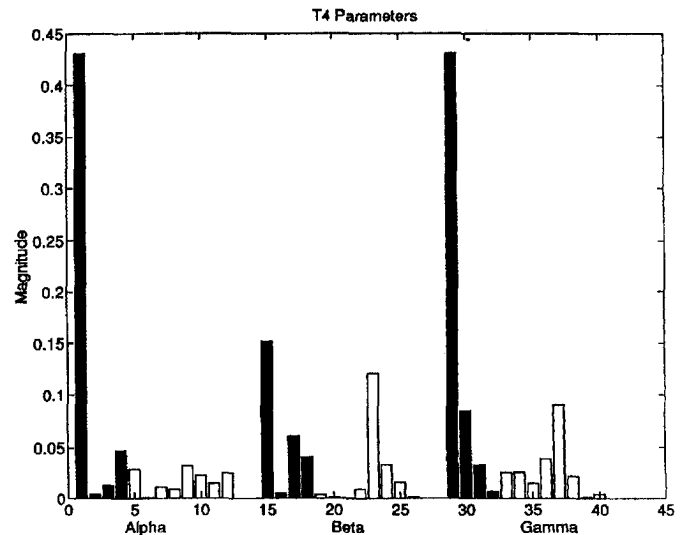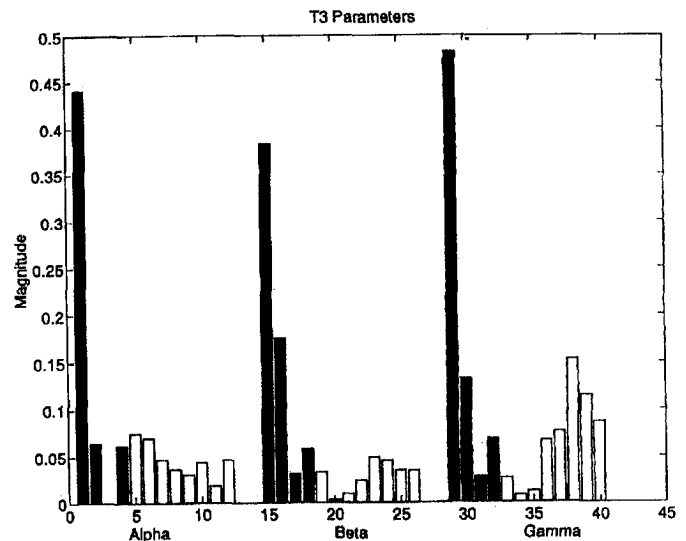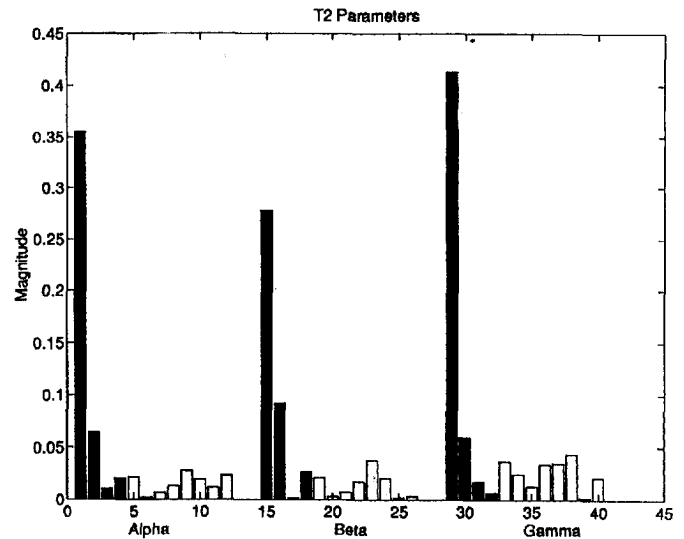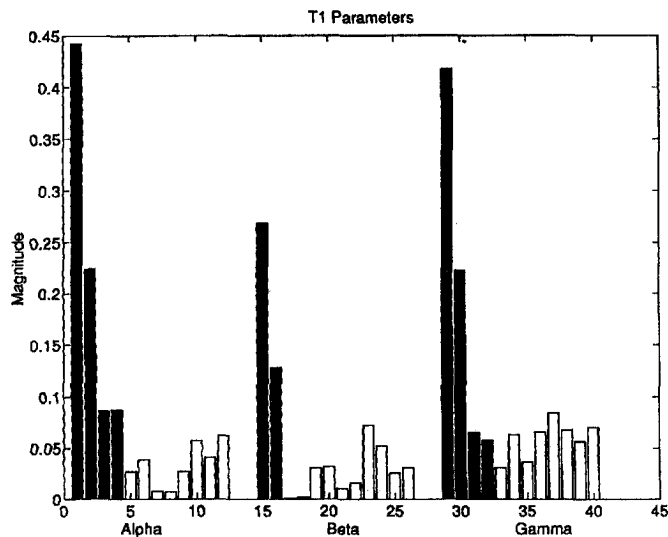
we used $\epsilon_\mu = 15$ for the mean test, $\epsilon_\sigma = 64$ for the covariance test, and a threshold of 50 for the log pseudolikelihood ratio test of (10). The neighborhood matrices were the same as for

the M_2 model described in Section IV.A. A value of $T = 200$ was used in conjunction with the stopping rule of (12). The performance of the algorithm was relatively insensitive to these parameter settings. To indicate boundaries of segmented regions in the processed images, we use different colors and widths of lines to optimize visibility. The images are of sizes ranging between 256 × 256 and 384 × 384 and initial block sizes were set to 16 × 16. During the process of display for reproduction, the original and processed images were magnified causing a somewhat blurry appearance in this paper.

Fig. 12 is an image of rocks in the sea. Fig. 13 is the result after the region splitting phase and Fig. 14 is the result after conservative merging. In this example, we observe a large amount of region splitting near texture boundaries and due to color variation within textured regions. In the conservative merging phase, the criteria are used to merge small segments with similar neighboring segments to form texture boundaries. The result of the final segmentation is shown in Fig. 15. Note that the different textures are accurately segmented including the separation of rock and shadow regions. Fig. 16 plots the pseudolikelihood ratio at each merge during the stepwise optimal merging process. Most of the peaks are concentrated near the 246th merge which completed the segmentation. The GMRF parameters for prominent regions in the segmented image are given in Table III. The associated bar graphs display the magnitude of the tabulated parameters with shaded bars indicating within-plane interactions.

Fig. 13. Result after the region splitting phase.

Fig. 14. Result after conservative merging.

Fig. 12. Image of rocks in the sea.

Fig. 15. Final segmentation.

Fig. 17 is an image of a scene containing a beach, water, grass, and dense foliage. Fig. 18 is the result following region splitting and Fig. 19 is the result after conservative merging. Due to a number of small features in the image, several small blocks remain after conservative merging. Figs. 20 and 21 show the result of agglomerative clustering at intermediate stages in the segmentation process and Fig. 22 is the final segmentation. Fig. 23 is a plot of the pseudolikelihood ratio during the segmentation. Each of the results shown in Figs. 20-22 occurs before a merge corresponding to a peak in this ratio. The final segmentation accurately separates the beach, water, grass, and dense foliage.
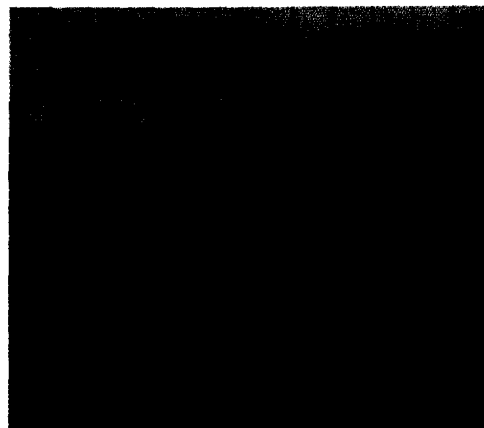
Fig. 16. Graph of the pseudolikelihood ratio at each merge.
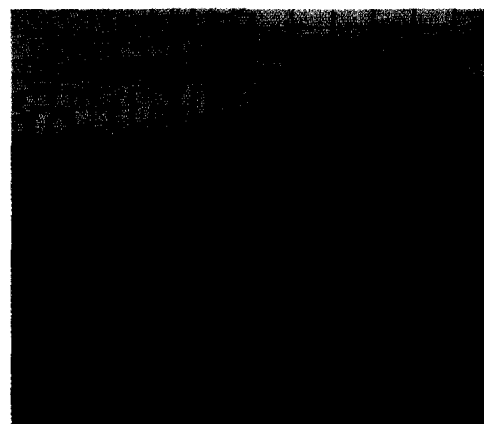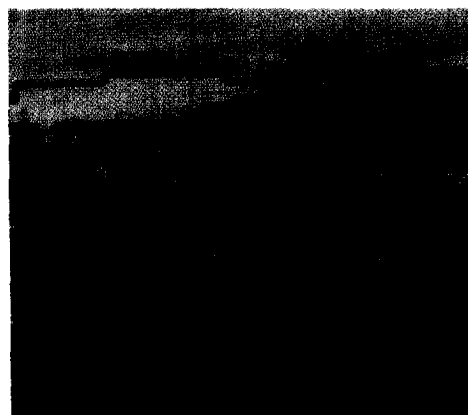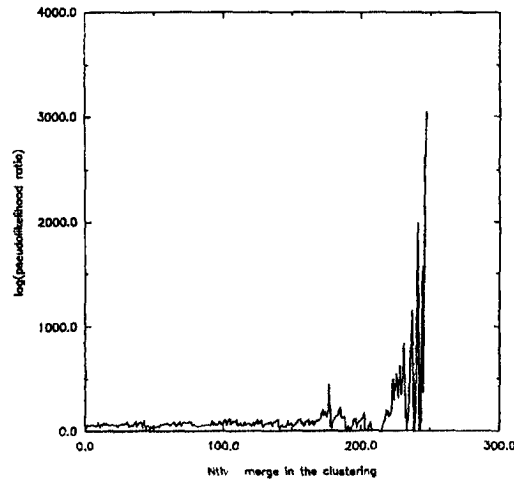

TABLE III
THE GMRF PARAMETERS FOR TEXTURES IN FIG. 12

| Parameter	Rock	Upper Sky	Lower Sky	Sea	Shadow
$\alpha_{RR}(1,0)$	0.5177	0.5194	0.5135	0.5285	0.5147
$\alpha_{RR}(0,1)$	0.5495	0.5960	0.5113	0.4749	0.4640
$\alpha_{RR}(1,1)$	-0.3003	-0.3185	-0.2669	-0.2657	-0.2527
$\alpha_{RR}(1,-1)$	-0.2682	-0.2993	-0.2585	-0.2364	-0.2223
$\alpha_{RG}(1,0)$	-0.0464	-0.0182	-0.0189	-0.0121	-0.00667
$\alpha_{RG}(0,1)$	0.0602	-0.0242	-0.0110	0.0622	0.0076
$\alpha_{RG}(1,1)$	-0.0100	0.0104	0.0188	-0.0107	-0.0024
$\alpha_{RG}(1,-1)$	-0.0121	0.0325	0.0084	-0.0399	0.00101
$\alpha_{RB}(1,0)$	0.0251	0.0285	0.0495	0.0211	0.0287
$\alpha_{RB}(0,1)$	-0.0267	0.1501	0.0560	0.0570	0.0762
$\alpha_{RB}(1,1)$	0.0081	-0.0801	-0.0551	-0.0480	-0.0416
$\alpha_{RB}(1,-1)$	-0.0102	-0.0986	-0.0506	-0.0356	-0.0667
$\beta_{GG}(1,0)$	0.4989	0.5203	0.5031	0.4936	0.5034
$\beta_{GG}(0,1)$	0.5388	0.5216	0.4240	0.50076	0.4140
$\beta_{GG}(1,1)$	-0.2675	-0.2804	-0.2161	-0.2417	-0.2158
$\beta_{GG}(1,-1)$	-0.2684	-0.2629	-0.2118	-0.2530	-0.1997
$\beta_{GR}(1,0)$	0.0020	-0.0072	-0.0026	0.02185	0.0003
$\beta_{GR}(0,1)$	0.0938	0.00515	0.0125	0.0498	0.0100
$\beta_{GR}(1,1)$	-0.0342	-0.0049	0.0096	-0.0307	0.0009
$\beta_{GR}(1,-1)$	-0.0236	0.0067	-0.0198	-0.0405	-0.0136
$\beta_{GB}(1,0)$	0.0247	0.0202	0.0356	0.0208	0.03590
$\beta_{GB}(0,1)$	-0.0325	0.0568	0.0921	0.05527	0.1253
$\beta_{GB}(1,1)$	0.0031	-0.0317	-0.0783	-0.0562	-0.0842
$\beta_{GB}(1,-1)$	0.0020	-0.0459	-0.0503	-0.02489	-0.0793
$\gamma_{BB}(1,0)$	0.5210	0.5308	0.5256	0.4914	0.5008
$\gamma_{BB}(0,1)$	0.4053	0.5350	0.3914	0.4469	0.3617
$\gamma_{BB}(1,1)$	-0.2116	-0.2955	-0.219	-0.2429	-0.1577
$\gamma_{BB}(1,-1)$	-0.2151	-0.2701	-0.1968	-0.1965	-0.2013
$\gamma_{BR}(1,0)$	0.0100	0.0050	0.0137	0.0418	0.0241
$\gamma_{BR}(0,1)$	0.0833	0.1920	0.1139	0.0603	0.0831
$\gamma_{BR}(1,1)$	-0.0543	-0.1387	-0.0849	-0.0456	-0.0626
$\gamma_{BR}(1,-1)$	-0.0418	-0.1107	-0.0741	-0.0577	-0.0497
$\gamma_{BG}(1,0)$	-0.0079	0.00211	-0.0025	0.0007	0.0049
$\gamma_{BG}(0,1)$	0.0689	-0.0086	0.0536	0.0824	0.0974
$\gamma_{BG}(1,1)$	-0.0299	-0.0064	-0.0288	-0.0315	-0.0653
$\gamma_{BG}(1,-1)$	-0.0303	0.0126	-0.0256	-0.0537	-0.0376
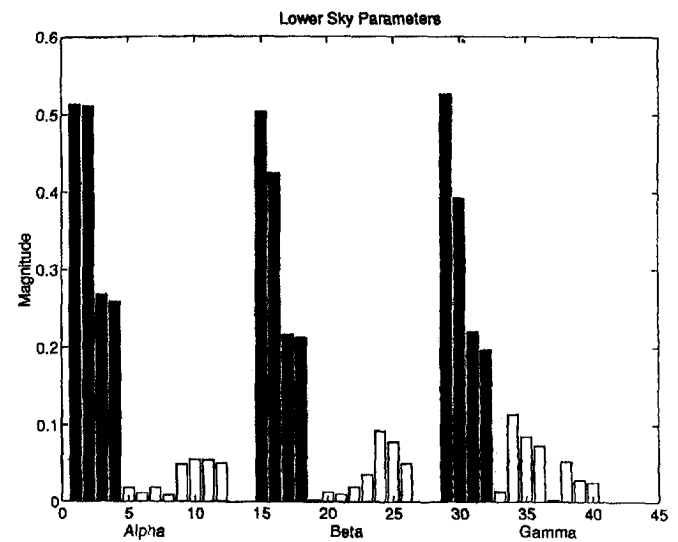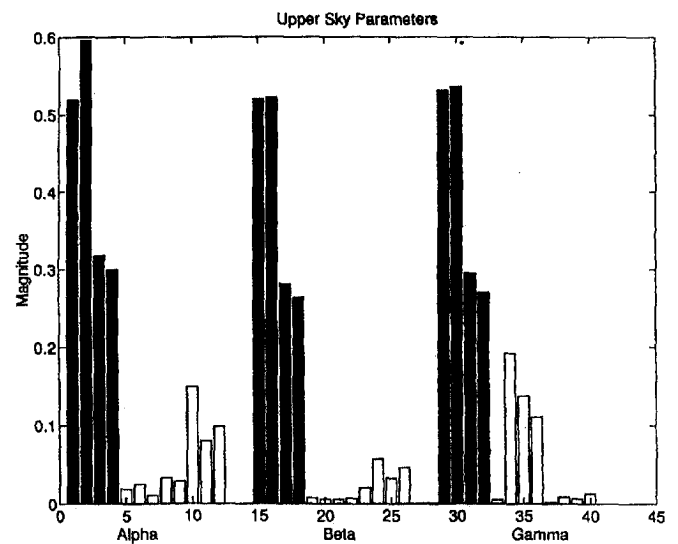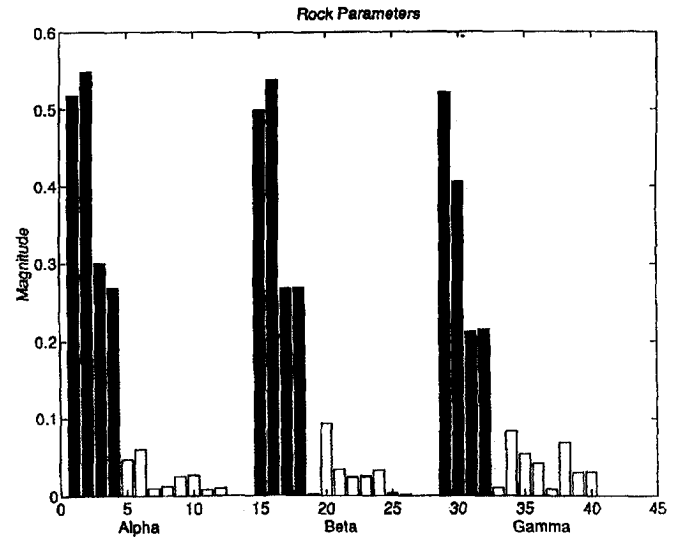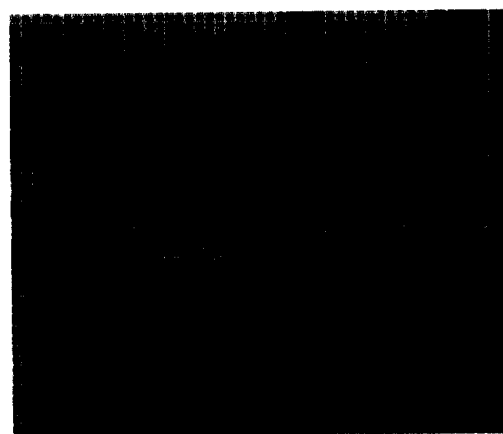
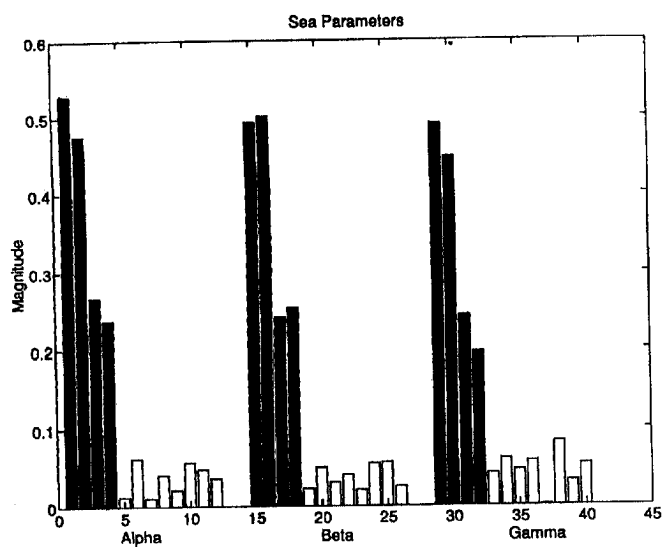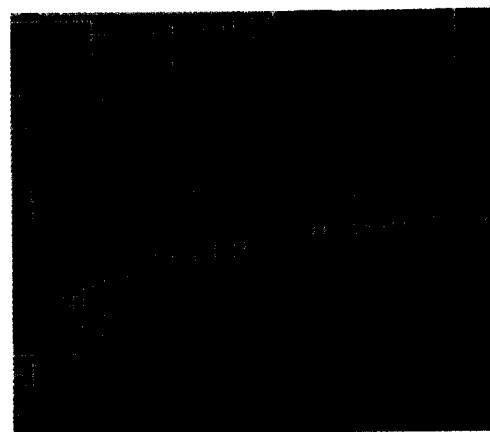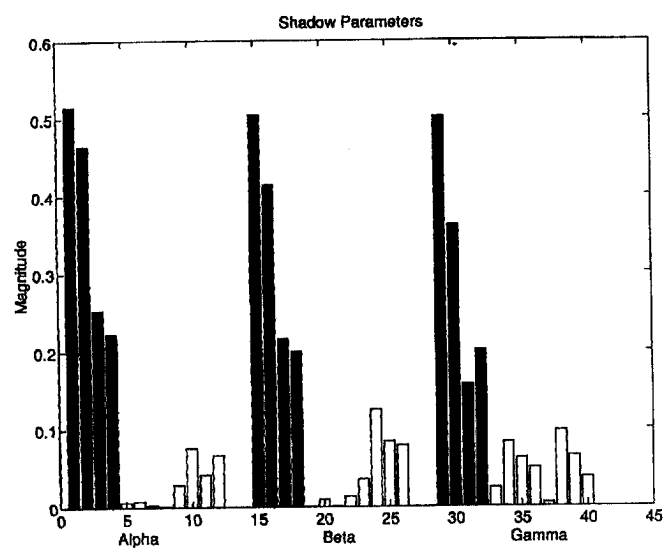Fig. 18. Result after the region splitting phase.

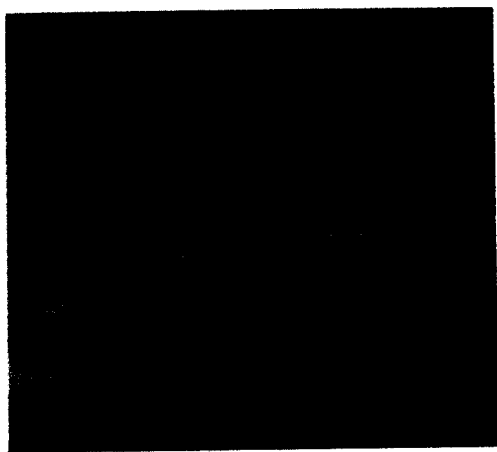Fig. 19. Result after conservative merging.

Fig. 20 Result after merge 137 during stepwise optimal merging.

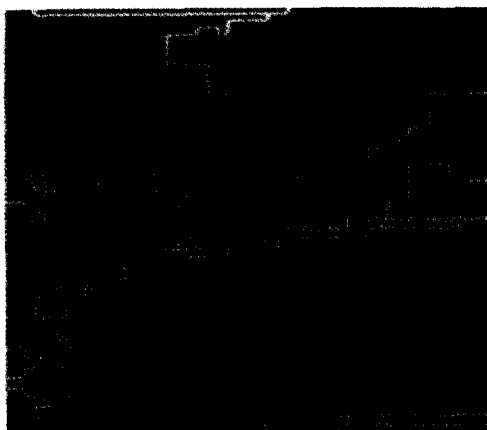Fig. 17. Image of a beach, water, and foliage.

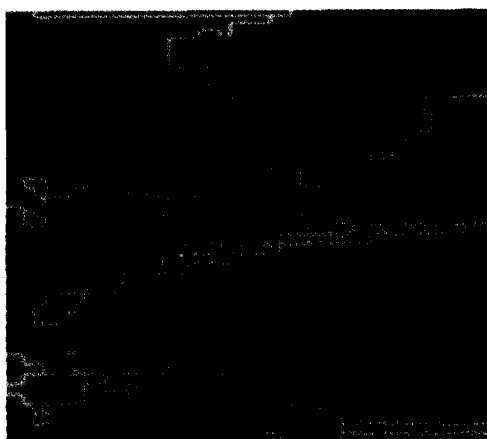Fig. 21. Result after merge 157 during stepwise optimal merging.
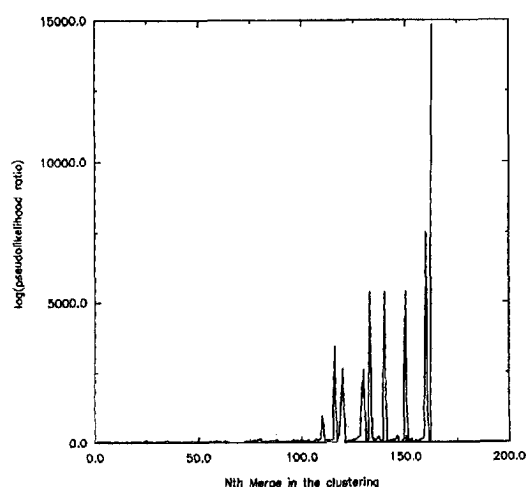

Fig. 22. Final segmentation.

Fig. 23. Graph of the pseudolikelihood ratio at each merge.

Fig. 24 is an image of a beach scene with the ocean, sand, and a person. Fig. 25 is the result after region splitting. Since the color textures have significant spatial variation over much of the image, many small blocks are formed as a result of the splitting. Fig. 26 is the result following conservative merging

which significantly reduces the total number of image segments in preparation for stepwise optimal merging. Fig. 27 is the final segmentation which partitions the image into ocean, sand, and person. Note that while the person consists of both skin tones and darker regions, the stopping rule used for these experiments allows the merger of these small components into a single region. If different stopping rule parameters are chosen, the segmentation may be terminated before these small regions are merged.

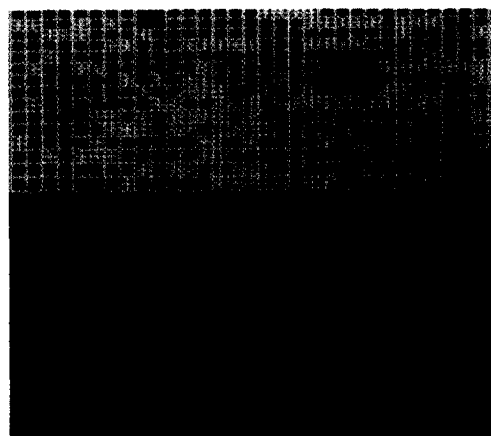Fig. 24. Image of a beach scene.

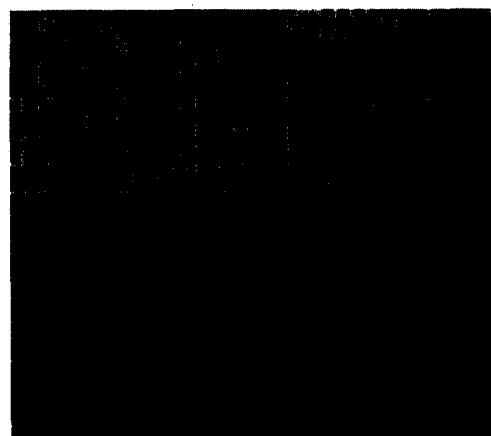
Fig. 25. Result after the region splitting phase.

Fig. 26. Result after conservative merging.

Fig. 27. Final segmentation.

Fig. 28 is an image of an umbrella and a tree. Fig. 29 is the result following region splitting and Fig. 30 is the result following conservative merging. The final segmentation is presented in Fig. 31. The algorithm accurately separates the tree texture from the umbrella texture and partitions the umbrella into an illuminated and shadowed component.
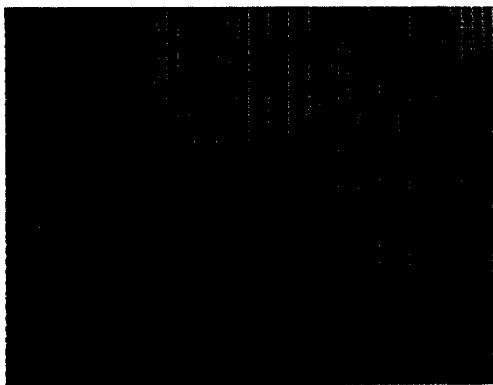

Fig. 28. Image of an umbrella and a tree.

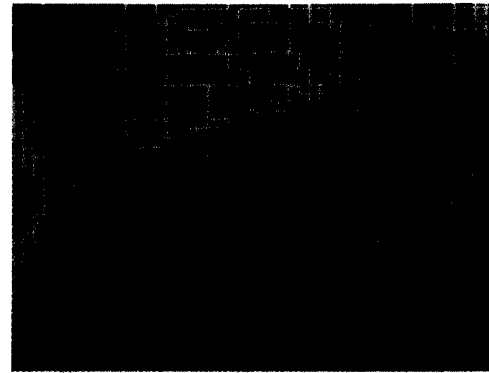Fig. 29. Result after the region splitting phase.
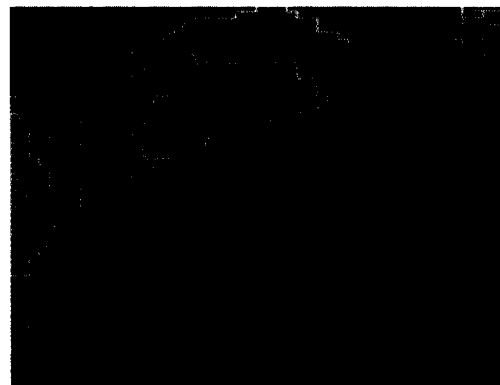

Fig. 30. Result after conservative merging.

Fig. 31. Final segmentation.

V. CONCLUSION

We have introduced a Markov random field model for color texture that captures spatial interaction within and between the bands of a color image. An unsupervised segmentation algorithm has been designed that uses this model with an efficient maximum pseudolikelihood scheme for estimating model parameters from image regions. The final stage of the segmentation algorithm is a stepwise optimal merging process that at each iteration selects a merge that maximizes the conditional pseudolikelihood of the image. The effectiveness of the model and algorithm have been demonstrated on many color images of natural scenes with examples presented showing the importance of considering the full GMRF color texture model proposed in Section II.A.

An important problem that has not been addressed in this paper is the selection of neighbors during the design of color random field models. This selection is of particular importance for color images because of the large number of possible parameters that can be used to define interactions within and between color bands. In [23], we present a Bayesian method for selecting neighbors in spatial interaction models for color images which generalizes previous approaches used for intensity images. The results in [23] suggest that domain knowledge about a class of images can be used to improve the effectiveness of color random field models used during segmentation.

APPENDIX A
ESTIMATION OF GMRF PARAMETERS USING THE PSEUDOLIKELIHOOD

We present a set of linear equations that is solved for the maximum likelihood α, β, and γ parameter estimates using the pseudolikelihood model of (7) under the assumption that the covariance matrix Σ_S is diagonal as described in III.B.1. Let M_S be the number of pixels in region S, and let $q(i, j) = R(i, j) - \mu_R$, $t(i, j) = G(i, j) - \mu_G$, $s(i, j) = B(i, j) - \mu_B$, and let $q_{mn}(i, j) = R(i + m, j + n) - \mu_R$, $t_{mn}(i, j) = G(i + m, j + n) - \mu_G$, and $s_{mn}(i, j) = B(i + m, j + n) - \mu_B$. Maximizing (7) by differentiating with respect to each of the GMRF parameters results in separate sets of linear equations for the α, β, and γ parameters. For example, the system below can be solved for the vector of α parameters.

$$\sum_{(i,j)\in S} \begin{bmatrix} q_{10}^2 & q_{10}q_{01} & \cdots & q_{10}s_{10} & \cdots \\ q_{01}q_{10} & q_{01}^2 & \cdots & q_{01}s_{10} & \cdots \\ q_{mn}q_{10} & q_{mn}q_{01} & \cdots & q_{mn}s_{10} & \cdots \\ \cdots & \cdots & \cdots & \cdots & \cdots \\ t_{10}q_{10} & t_{10}q_{01} & \cdots & t_{10}s_{10} & \cdots \\ \cdots & \cdots & \cdots & \cdots & \cdots \\ s_{10}q_{10} & s_{10}q_{01} & \cdots & s_{10}^2 & \cdots \\ \cdots & \cdots & \cdots & \cdots & \cdots \end{bmatrix} \begin{bmatrix} \alpha_{RR}(1, 0) \\ \alpha_{RR}(0, 1) \\ \alpha_{RR}(m, n) \\ \cdots \\ \alpha_{RG}(1, 0) \\ \cdots \\ \alpha_{RB}(1, 0) \\ \cdots \end{bmatrix} = \sum_{(i,j)\in S} \begin{bmatrix} qq_{10} \\ qq_{01} \\ qq_{mn} \\ \cdots \\ qt_{10} \\ \cdots \\ qs_{10} \\ \cdots \end{bmatrix} \quad (15)$$

where as indicated the q, s, and t parameters are summed over (i, j) so that, for example, $q_{01}q_{10}$ refers to $q_{01}(i, j)q_{10}(i, j)$. The element v_{rr} of Σ_S is computed by substituting the estimated α parameters into (3) and using

$$v_{rr} = \frac{1}{M_S} \sum_{(i,j)\in S} \left(e_r(i, j)^2 \right) \quad (16)$$

Equations similar to (15) can be solved for the estimation of the β and γ parameters. The variances v_{gg} and v_{bb} are estimated using the β and γ parameters in a manner similar to (16).

APPENDIX B
COMPUTING THE PSEUDOLIKELIHOOD RATIO

From (7), the log of the pseudolikelihood of a segment S of size M_S pixels is given by

$$-M_S \ln\left(8\pi^3\right) - \frac{1}{2} M_S \ln\left(|\Sigma_S|\right)$$

$$+ \sum_{(i,j)\in S} \left\{ -\frac{1}{2}\left[e_r(i, j)e_g(i, j)e_b(i, j)\right]\Sigma_S^{-1}\left[e_r(i, j)e_g(i, j)e_b(i, j)\right]^t \right\} \quad (17)$$

Assuming Σ_S is diagonal and substituting the estimates v_{rr}, v_{gg}, and v_{bb} of (16) into (17) for the elements of Σ_S gives

$$\ln\left(P_{ps}\left(S | \theta_S, \Sigma_S\right)\right) = -M_S \ln\left(8\pi^3\right) - \frac{1}{2} M_S \ln\left(|\Sigma_S|\right) - \frac{3}{2} M_S \quad (18)$$

Considering the merge of a segment S_k of size D_k pixels with a segment S_l of size D_l pixels gives the pseudolikelihood ratio

$$h(k, l) = \ln\left(R_{ps}(k, l)\right) = \frac{(D_k + D_l)}{2} \ln\left(|\Sigma_{S_M}|\right) - \frac{D_k}{2} \ln\left(|\Sigma_{S_k}|\right) - \frac{D_l}{2} \ln\left(|\Sigma_{S_l}|\right) \quad (19)$$

stated in (10).

REFERENCES

[1] R. Bajcsy, S.W. Lee, and A. Leonardis, "Color image segmentation with detection of highlights and local illumination induced by inter-reflections," *Proc. Int'l Conf. Pattern Recognition*, pp. 785-790, Atlantic City, N.J., 1990.

[2] J.M. Beulieu and M. Goldberg, "Hierarchy in picture segmentation: A stepwise optimization approach," *IEEE Trans. Pattern Analysis and Machine Intelligence*, vol. 11, no. 2, pp. 150-163, Feb. 1989.

[3] J. Besag, "Spatial interaction and the statistical analysis of lattice systems," *J. Royal Statistical Society B*, vol. 36, pp. 192-236, 1974.

[4] R. Chellappa, S. Chatterjee, and R. Bagdazian, "Texture synthesis and compression using Gaussian-Markov random field models," *IEEE Trans. Systems, Man, and Cybernetics*, vol. 8, no. 2, pp. 298-303, Mar.-Apr. 1985.

[5] R. Chellapa, J.-H. Hu, and S.-Y. Kung, "On two-dimensional Markov spectral estimation," *IEEE Trans. Acoustics, Speech, and Signal Processing*, vol. 31, no. 4, pp. 836-841, 1983.

[6] P.C. Chen and T. Pavlidis, "Image segmentation as an estimation problem," *Computer Graphics and Image Processing*, vol. 12, pp. 153-172, 1980.

[7] F. Cohen, "Markov random fields for image modeling and analysis," U. Desai, ed., *Modeling and Application of Stochastic Processes*, pp. 243-272. Boston: Kluwer Academic, 1986.

[8] F. Cohen and Z. Fan, "Maximum likelihood unsupervised textured image segmentation," *Computer Vision, Graphics, and Image Processing: Graphical Models and Image Processing*, vol. 54, no. 3, pp. 239-251, 1992.

[9] D. Cooper, "Stocahstic boundary estimation and object recognition," *Computer Graphics and Image Processing*, pp. 326-355, Apr. 1980.

[10] M. Daily, "Color image segmentation using Markov random fields," *Proc. IEEE Conf. Computer Vision and Pattern Recognition*, pp. 304-312, 1989.

[11] A. Gagalowicz, S.D. Ma, and C. Tournier-Lasserve, "Efficient models for color textures," *Proc. Eighth Int'l Conf. Pattern Recognition*, pp. 412-414, 1986.

[12] S. Geman and D. Geman, "Stochastic relaxation, Gibbs distributions, and the Bayesian restoration of images," *IEEE Trans. Pattern Analysis and Machine Intelligence*, vol. 6, no. 6, pp. 721-741, Nov. 1984.

[13] G. Healey, "Segmenting images using normalized color," *IEEE Trans. Systems, Man, and Cybernetics*, vol. 22, pp. 64-73, Jan. 1992.

[14] G. Healey, S.A. Shafer, and L.B. Wolff, eds., *Physics-Based Vision: Principles and Practice, COLOR*. Jones and Barlett, 1992.

[15] R. Kashyap and R. Chellappa, "Estimation and choice of neighbors in spatial interaction models of images," *IEEE Trans. Information Theory*, vol. 29, no. 1, pp. 60-72, Jan. 1983.

[16] R. Kashyap, R. Chellappa, and N. Ahuja, "Decision rules for choice of neighbors in random field models of images," *Computer Graphics and Image Processing*, vol. 15, no. 1, pp. 301-318, 1981.

[17] G.J. Klinker, S.A. Shafer, and T. Kanade, "A physical approach to color image understanding," *Int'l J. Computer Vision*, vol. 4, pp. 7-38, 1990.

[18] S. Lakshmanan and H. Derin, "Simultaneous parameter estimation and segmentation of Gibbs random fields using simulated annealing," *IEEE Trans. Pattern Analysis and Machine Intelligence*, vol. 11, pp. 799-813, Aug. 1989.

[19] W.E. Larimore, "Statistical interaction and statistical analysis of lattice systems," *Proc. IEEE*, vol. 65, pp. 961-970, 1977.

[20] B.S. Manjunath and R. Chellappa, "Unsupervised texture segmentation using Markov random field models," *IEEE Trans. Pattern Analysis and Machine Intelligence*, vol. 13, no. 5, pp. 478-482, May 1991.

[21] Y. Ohta, T. Kanade, and T. Sakai, "Color information for region segmentation," *Computer Graphics and Image Processing,* vol. 13, pp. 222-241, 1980.

[22] D. Panjwani, "Segmentation of textured color images," Master's thesis, Dept. of Electrical and Computer Eng., Univ. of California, Irvine, 1993.

[23] D. Panjwani and G. Healey, "Selecting neighbors in random field models for color images," *Proc. First IEEE Int'l Conf. Image Processing,* Austin, Tex., 1994.

[24] T. Pavlidis, *Structural Pattern Recognition.* Springer-Verlag, 1991.

[25] T. Poggio, E. Gamble, and J. Little, "Parallel integration of vision modules," *Science,* vol. 242, pp. 436-440, Oct. 1988.

[26] J. Scharcanski, J.K. Hovis, and H.C. Shen, "Color texture representation using multiscale feature boundaries," *SPIE Vol. 1818 Visual Communications and Image Processing,* pp. 156-165, 1992.

[27] J. Silverman and D. Cooper, "Bayesian clustering for unsupervised estimation of surface and texture models," *IEEE Trans. Pattern Analysis and Machine Intelligence,* vol. 10, no. 4, pp. 482-495, July 1988.

[28] J. Woods, "Two dimensional discrete Markov random fields," *IEEE Trans. Information Theory,* vol. 18, pp. 232-240, 1972.

[29] W. Wright, "A Markov random field approach to data fusion and color segmentation," *Image and Vision Computing,* vol. 7, pp. 144-150, 1989.

[30] Y. Yakimovsky, "Boundary and object detection in real world images," *J. ACM,* vol. 23, pp. 599-618, 1976.

Dileep Kumar Panjwani received the BTech degree in electrical engineering from the Indian Institute of Technology, Delhi, India, in 1991 and the MS degree from the University of California, Irvine, in 1993. He is currently working at Mentor Graphics Corporation. His interests include segmentation and modeling of color images and hardware synthesis for image processing applications.

Glenn Healey received the BSE degree in computer engineering from the University of Michigan, Ann Arbor, in 1984, and the MS degree in computer science, the MS degree in mathematics, and the PhD degree in computer science from Stanford University in 1985, 1986, and 1988, respectively.

From 1984 to 1989 Dr. Healey was affiliated with the Computer Science Department, IBM Almaden Research Center as a research student associate and visiting scientist. In 1989 he joined the Electrical and Computer Engineering Department at the University of California, Irvine, where he is currently an associate professor. His research interests in machine vision and image processing include physical modeling of visible and infrared image formation, algorithm development and characterization, and high-performance architectures.